Finite-difference modeling of marine vibrator sources

Khalid Almuteri, Jeffrey Shragge & Paul Sava
Center for Wave Phenomena and Dept. of Geophysics, Colorado School of Mines, Golden CO 80401
email kalmuteri@mines.edu

ABSTRACT
Marine vibrators are emerging as an attractive alternative to conventional air-guns in ocean-bottom acquisition due to their ability to generate low-frequency waves and to limit negative impacts on marine wildlife. Using marine vibrators introduces challenges not found in conventional air-gun-based acquisition, including handling phenomena associated with the Doppler effect due to the source motion and time-dependent source-receiver offsets when receivers are placed on the ocean bottom. Standard seismic data processing solutions assume stationary sources and receivers; however, accurately accounting for source motion effects in processing is critical for optimal subsurface imaging. To address these challenges, we develop a finite-difference approach for modeling full acoustic wavefields in a generalized coordinate system that tracks the moving source. Synthetic examples demonstrate that this technique has the ability to accurately and stably model high-velocity moving sources, and account for the wavefield distortion predicted by Doppler theory. This approach is not limited to understanding wavefield propagation for a moving source and can be used to develop other advanced processing techniques for marine vibrator data.

Key words: Marine vibrator, modeling, marine acquisition

1 INTRODUCTION

Environmental concerns about conventional marine impulsive sources (i.e., air-guns) make a transition to environmentally friendly marine vibrators likely in the near future. Non-impulsive marine sources (i.e., marine vibrators) are viable alternatives to air-guns. They are not just advantageous for environmental reasons, but also have geophysics-related merits. From a seismic exploration perspective, marine vibrators provide more low-frequency content than air-guns (Guitton et al., 2021), and enable simultaneous acquisition by blending phase-encoded sources (Laws et al., 2019). However, processing and imaging challenges emerge because of the motion and long duration of the marine vibrator signal, including Doppler effects and time-dependent source-receiver offsets in ocean-bottom acquisition. Even though marine vibrators move at a much slower velocity than the subsurface sound speed, source motion introduces a noticeable offset- and time-dependent frequency shift to the data (Dragoset, 1988; Schultz et al., 1989; Hampson and Jakubowicz, 1995). Further, phase distortion also occurs in seismic signals and is proportional to the source velocity and time slope of seismic events.

Current seismic data processing workflows usually assume stationary and impulsive sources in marine acquisition. Developing appropriate processing workflows for data acquired using moving sources requires accurate modeling of the associated effects. Numerical solutions to the wave equation form the basis of many geophysical applications such as imaging and inversion, and are necessary to study and understand wave propagation under realistic acquisition conditions (e.g., dynamic sea surfaces and/or moving sources). Further, numerical solutions assist in designing proper processing workflows and are necessary to validate processing solutions. Accurate modeling of seismic wavefields remains a key element in advanced seismic imagining and inversion techniques, such as reverse-time migration (RTM) and full-waveform inversion (FWI). Various methods are proposed in the literature to model marine vibrator data. Dellinger and Díaz (2020) present a segmentation-deconvolution approach to model mobile sources. JafarGandomi and Grion (2021) model marine vibrator data by interpolating unaliased impulsive sources data to desired source locations and convolving with the vibrator sweep. Duquet et al. (2021) use finite differences (FD) to model source motion by moving and interpolating the source injection locations in space as a function of time. Conventional Cartesian-based modeling methods are susceptible to numerical instabilities and modeling inaccuracies when introducing irregular or dynamic computational

geometries (e.g., time-varying sea surfaces). More challenges arise when implementing free-surface boundary conditions for such irregular geometries in a Cartesian coordinate system.

In this paper, we present a finite-difference approach to model the full acoustic wavefield triggered by a mobile source in a generalized coordinate system that effectively embeds source motion into the coefficients of the governing tensorial acoustic wave equation. Shragge (2014) and Shragge and Tapley (2017) present a time-invariant tensorial representation of the acoustic wave equation (AWE) in a generalized coordinate system. This approach facilitates coordinate transformation to map the irregular physical domain to a regular computational domain, enabling FD modeling. Konuk and Shragge (2020) extend this technique to address the challenge of dynamic sea surfaces by specifying a time-variant 4D coordinate transformation. This extension leads to a time-varying mesh grid in physical Cartesian coordinates, but a stationary mesh grid in a generalized computational coordinate system.

Here, we solve the AWE for a time-varying mesh without a need for repeated velocity model interpolation, eliminating the added computational complexity and accuracy issues associated with this operation. In this framework, the time-varying physical Cartesian domain horizontally shears conformal with source motion. However, the computational domain is fixed in time with time- and space-dependent partial differential operator coefficients. The developed approach is not limited to modeling moving sources with ocean-bottom receivers, and is applicable for conventional towed-streamer scenarios.

2 THEORY

2.1 Tensorial acoustic wave equation

The 4D tensorial AWE in a generalized coordinate system defined by the variables $\boldsymbol{\xi} = \left[\xi^0, \xi^1, \xi^2, \xi^3\right]$ is (Konuk and Shragge, 2020)

$$\Box_\xi P_\xi = F_\xi, \tag{1}$$

where $\Box_\xi$ is the generalized d'Alembert operator, P_ξ is the pressure field, and F_ξ is the source function. The ξ^0 coordinate is time and ξ^1, ξ^2, ξ^3 are space components. The generalized d'Alembert operator is

$$\Box_\xi = \frac{-1}{\sqrt{|\boldsymbol{g}|}} \frac{\partial}{\partial \xi^\mu} \left(\sqrt{|\boldsymbol{g}|} g^{\mu\nu} \frac{\partial}{\partial \xi^\nu} \right), \; \mu, \nu = 0, \cdots, 3, \tag{2}$$

where $[g^{\mu\nu}]$ is a symmetric rank-two contravariant metric tensor, $|\boldsymbol{g}|$ is the determinant of the covariant metric tensor $[g^{\mu\nu}]$, and $[g_{\mu\nu}] = [g^{\mu\nu}]^{-1}$. Here, we use superscript indices for components with a contravariant representation, and subscript indices for components with a covariant representation. In Cartesian coordinates with variables $\boldsymbol{x} = \left[x^0, x^1, x^2, x^3\right] = [t, x, y, z]$, the d'Alembert operator (equation 2) reduces to

$$\Box = \frac{-1}{c^2} \frac{\partial^2}{\partial t^2} + \nabla^2, \tag{3}$$

where $c = c(\boldsymbol{x})$ is the Cartesian medium velocity, and ∇^2 is the 3D Cartesian Laplacian operator. The covariant metric tensor relates the generalized coordinate geometry to an equivalent Cartesian coordinate system representation with elements given by

$$g_{\mu\nu} = \frac{\partial x^i}{\partial \xi^\mu} \frac{\partial x^i}{\partial \xi^\nu} \quad \text{for} \quad i, \mu, \nu = 0, \cdots, 3, \tag{4}$$

where repeated indices imply summation. The columns of the contravariant and covariant metric tensors form dual bases (i.e., the dot product $\langle \boldsymbol{g}_i \; , \; \boldsymbol{g}^j \rangle = \delta_{ij}$).

To simulate wavefields triggered by a moving source, we set the generalized AWE in arbitrary coordinates and then choose a coordinate transformation that maps a horizontally deformed physical domain to a regular computational domain. To simplify the 4D coordinate transformation, we make a set of plausible assumptions: (1) no stretching of the time coordinate occurs, i.e. $x^0 = \xi^0$ (or $t = \tau$); (2) the horizontal source movement is along the ξ^1-axis only, leaving the ξ^2-axis unchanged (i.e., $x^2 = \xi^2$); (3) the source moves at a fixed depth level (i.e., there is no vertical motion and thus $x^3 = \xi^3$); (4) the source moves at a constant velocity (i.e., $\frac{\partial v}{\partial \xi^0} = 0$); and (5) the source moves in a homogeneous fluid medium. The first four assumptions allow us to express the horizontal mesh deformation $x^1 = T\left(\xi^0, \xi^1, \xi^2, \xi^3\right)$, where T is any arbitrary horizontal deformation function that depends on all variables $\left(\xi^0, \xi^1, \xi^2, \xi^3\right)$. Recognizing that $\xi^0 \equiv c\tau$ and $\frac{\partial}{\partial \xi^0} = \frac{1}{c} \frac{\partial}{\partial \tau}$, the generalized d'Alembert operator (equation 2) for an arbitrarily deformed mesh along the ξ^1-axis reduces to the second-order AWE

$$\frac{1}{T_1} \frac{\partial}{\partial \tau} \left(\frac{T_1}{c^2} \frac{\partial P_\xi}{\partial \tau} \right) = \frac{1}{T_1} \left[\frac{\partial}{\partial \xi^1} \left(\frac{T_0}{c} \frac{\partial P_\xi}{\partial \tau} \right) + \frac{\partial}{\partial \tau} \left(\frac{T_0}{c} \frac{\partial P_\xi}{\partial \xi^1} \right) \right] + \frac{1}{T_1} \frac{\partial}{\partial \xi^i} \left(T_1 g^{ij} \frac{\partial P_\xi}{\partial \xi^j} \right) + F_\xi, \tag{5}$$

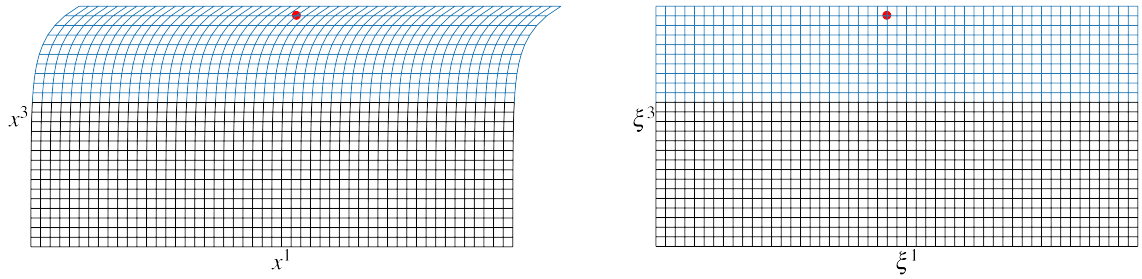

(a) (b)

Figure 1. (a) Physical and (b) computational domains. The red dot indicates the source location. The blue mesh represents a homogeneous region, whereas the black mesh represents a variable velocity region.

where $T_k = \frac{\partial T}{\partial \xi^k}$, and $i, j = 1, 2, 3$ are spatial indices. The assumptions stated above allow us to express the relationship between the $\boldsymbol{\xi}$- and $\boldsymbol{x}$-coordinate systems as

$$\begin{bmatrix} x^0 \\ x^1 \\ x^2 \\ x^3 \end{bmatrix} = \begin{bmatrix} \xi^0 \\ \xi^1 + v\xi^0 e^{\gamma(s_z - \xi^3)} \\ \xi^2 \\ \xi^3 \end{bmatrix}, \tag{6}$$

where v is the source velocity, γ is a user-defined decay factor that controls the amount of horizontal deformation as function of depth, and s_z is the source depth. By introducing a depth-dependent horizontal deformation, we confine the time-varying mesh deformation to the homogeneous water layer. This coordinate transformation enables the modeling of a moving source without the need for velocity model interpolation at each time-step. Figure 1a and 1b show a deformed physical domain in Cartesian coordinates and the fixed computational domain in a generalized coordinate system, respectively. At the initial time, the computational and physical domains are identical (i.e., $x^1 = \xi^1$). Extending this approach to include a moving source with a time-dependent velocity, i.e. $v \rightarrow v(\xi^0)$, is straightforward.

2.2 Doppler effect

In a constant velocity medium, the source motion causes time-dependent frequency shifts in the data given by

$$f(t) = \frac{c}{c - v\,cos(\theta(t))} f_\circ(t), \tag{7}$$

where $f(t)$ is the time-dependent observed frequency, c is the speed of sound in the medium, v is the source speed, $\theta(t)$ is the time-dependant angle between the source and receiver or a scatterer point (Figure 2a), and $f_\circ(t)$ is the time-dependent input frequency.

For heterogeneous media, the ray paths from sources to scattering points play a role in the amount of frequency shifts. To derive an expression for the frequency change due to source motion in heterogeneous media, we follow the formulation of Kolano (1978). We consider a moving source with velocity v and a stationary point in the subsurface (Figure 2b). We assume that the source at time $t = 0$ s is at S_1 and after a time interval Δt it is at S_2 ($\Delta t = \frac{\Delta x}{v}$). If the source emits two pulses, one at each location, the time delay between emitting these pulses is Δt. The ray paths the two pulses take to arrive at the same location R are P_1 and P_2, with the associated travel times T_1 and T_2, respectively. The time delay between the two pulses at R is

$$\Delta\tau = \Delta t + T_2 - T_1 = \Delta t - \Delta T, \tag{8}$$

where $\Delta T = T_1 - T_2$. Considering the source emitting continuously when moving from S_1 to S_2, and because the total number of emitted cycles matches the total number of observed cycles, we have

$$f_\circ \Delta t = f \Delta\tau, \tag{9}$$

where $f_\circ$ and f are the emitted and observed frequencies, respectively. Thus, the frequency shift is

$$\Delta f = \frac{\Delta T}{\Delta\tau} f_\circ = \frac{\Delta T}{\Delta t - \Delta T} f_\circ, \tag{10}$$

which reduces to

$$\Delta f \approx \frac{\Delta T}{\Delta t} f_\circ \tag{11}$$

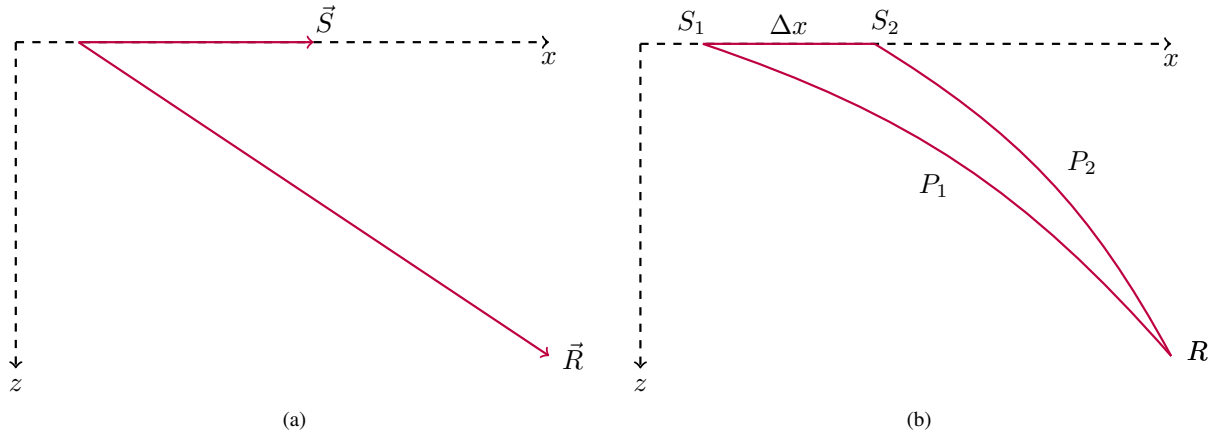

Figure 2. Schematic plot of (a) source motion direction ($\vec{S}$) relative to a stationary receiver or a scatterer point location ($\vec{R}$) in a constant velocity medium, and (b) a source moving from S_1 to S_2 with ray paths from source locations S_1 and S_2 to a point R in the subsurface is given by P_1 and P_2, respectively, in a variable velocity medium.

for $\frac{\Delta T}{\Delta t} \ll 1$, i.e. the source velocity is much slower than the speed of sound. As Δt approaches zero,

$$\Delta f = \lim_{\Delta t \to 0} \frac{T_2 - T_1}{\Delta t} f_\circ = \lim_{\Delta t \to 0} \frac{-\Delta T}{\Delta t} f_\circ = -\frac{dT}{dt} f_\circ. \tag{12}$$

Equation 12 shows that the Doppler effect in heterogeneous media is related to the material property along the ray path from the source to any point of interest in the subsurface. A more detailed treatment of the Doppler effect in complex media (e.g., anisotropic media) is commonly found in the physics literature concerning with radio waves propagating through the ionosphere (e.g., Weekes, 1958; Davies, 1965; Bennett, 1968).

3 NUMERICAL IMPLEMENTATION

We use a finite-difference approach to numerically solve the second-order acoustic wave equation (equation 5), i.e., using Taylor-expansion coefficients to approximate the partial differential operators. The numerical scheme uses approximations of order $O(\Delta\xi^2)$ for second-order partial differential operators and first-order spatial partial differential operators, and of order $O(\Delta\xi)$ for first-order temporal partial differential operators; however, using higher-order spatial approximations is possible. Implementing the second-order AWE permits modeling moving sources using a standard Cartesian-based AWE with relatively minor modifications. Synthetic examples show that the numerical scheme is stable and sufficiently accurate.

4 NUMERICAL EXAMPLES

4.1 Modeling in homogeneous media

In horizontally invariant media, one can set $\gamma = 0$ in equation 6, reducing the mesh deformation to a pure horizontal translation along the source motion direction. A positive (negative) velocity translates the mesh along the positive (negative) ξ^1 axis. To demonstrate the robustness of the developed approach and highlight the consequences of source motion on seismic data, we use an unrealistically fast source velocity of 0.5 km/s in a homogeneous medium. We simulate a 2D acoustic wavefield in a constant velocity medium of 1.5 km/s using a 20 Hz monochromatic sine wave. The source at time $t = 0$ s is at the location $x^1 = 2.0$ km (i.e., $\xi^1 = 2.0$ km). Figure 3a shows a snapshot at $t = 0.8$ s computed using the developed approach and interpolated to the Cartesian coordinate system. The right-going waves (i.e., along the source movement direction) are compressed, whereas the waves traveling in the opposite direction are dilated, according to the Doppler effect. The amount of compression or dilation is a function of the source velocity, the acoustic wavespeed in the medium, the source motion direction, the propagation direction, and the input frequency.

Figure 3b shows a shot gather recorded using stationary receivers placed 12.5 m below the source. The apices of the direct arrivals are shifted because of the source motion, and the lateral shift increases with time. Traces recorded to the right of the source

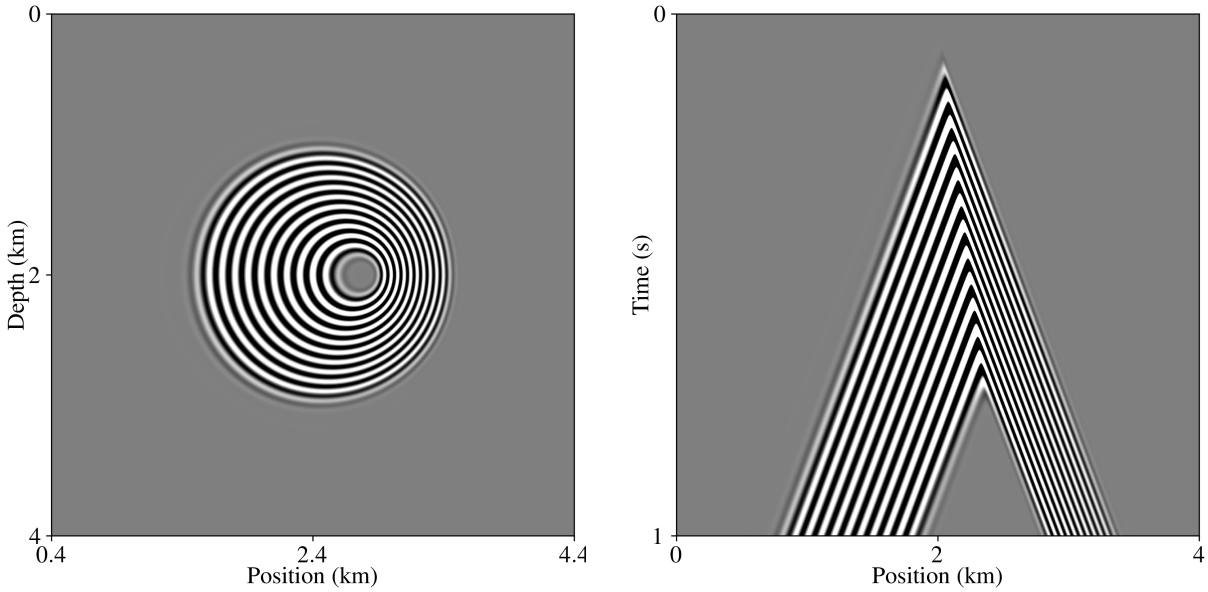

Figure 3. (a) Wavefield snapshot at $t = 0.8$ s. The left-going waves (opposite of the source movement direction) are dilated, whereas the right-going waves are compressed, demonstrating the Doppler effect due to source motion. (b) Shot gather of direct arrivals for stationary receivers located 12.5 m below the source.

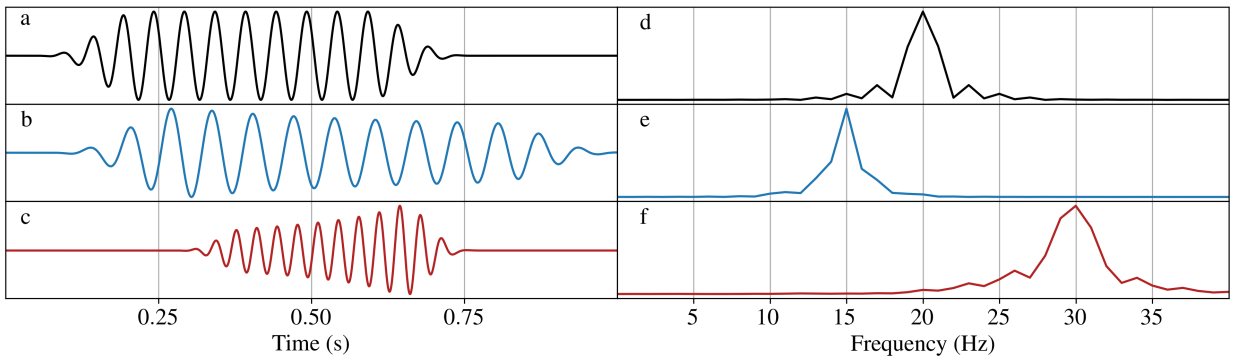

Figure 4. (a) Source function, and (b) and (c) are traces recorded at $x = 2.0$ km and $x = 2.37$ km, respectively. (d) Amplitude spectrum of the source function, and (e) and (f) amplitude spectra of the traces shown in (b) and (c), respectively.

are shifted to a higher frequency, while the traces recorded to the left of the source are shifted to a lower frequency. For a scattered wavefield, frequency shifts are independent of the receiver locations relative to the source. In other words, for a scattered wavefield due to a scatterer, frequency shifts are a function of source velocity and motion relative to the scatterer point.

Figures 4b and 4c show two traces for stationary receivers at $x^1 = 2.0$ km and $x^1 = 2.37$ km, respectively. Although the input source (Figure 4a) is a 20 Hz monochromatic wave (Figure 4d), the trace to the right of the source is compressed compared to that to the left. The amplitude spectra of the two traces (Figures 4b and 4c) indicate that the observed frequency at the right receiver is ~ 30 Hz, whereas the observed frequency at the left receiver is ~ 15 Hz. The theoretical observed frequencies using the Doppler (1842) formula agree with our numerical results.

4.2 Modeling in heterogeneous media

To examine source motion effects on seismic acquisition in heterogeneous media, we simulate the acoustic wavefield using the Marmousi II model. We use a source located at $[\xi^1, \xi^3] = [8.0, 0.0125]$ km and 721 receivers at $\xi^3 = x^3 = 0.5$ km with a

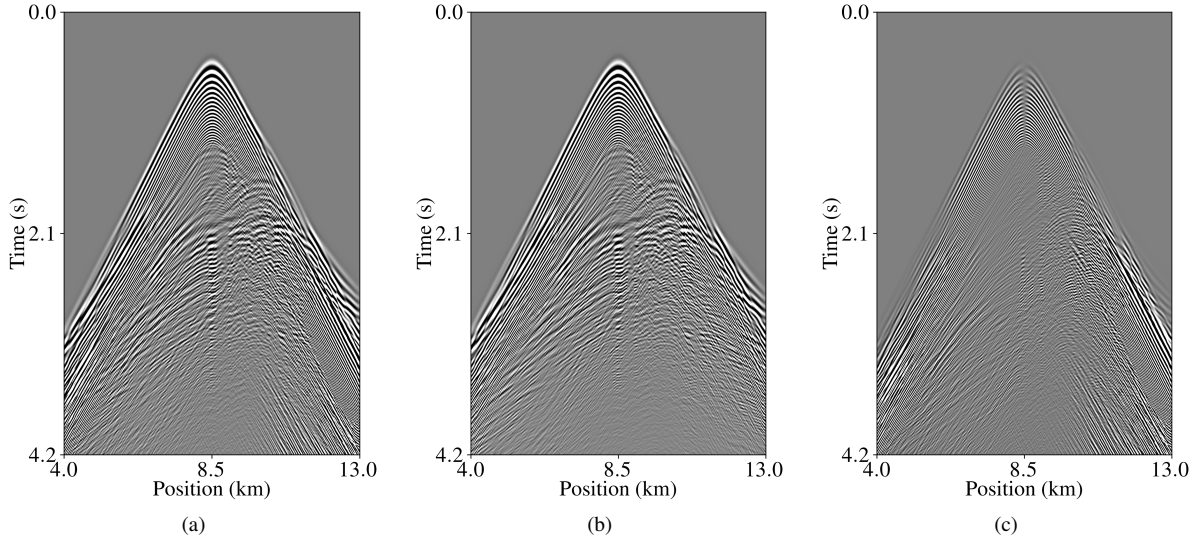

Figure 5. Shot gather acquired using (a) moving and (b) stationary sources. (c) Difference between the data shown in (a) and (b).

uniform 12.5 m spacing. We use a fast source velocity of 25 m/s to emphasize the discrepancies between a stationary and a moving source. The source function is a linear sweep from 16 Hz to 34 Hz. Figure 5a and 5b show shot gathers acquired using moving and stationary sources, respectively. As expected, the source motion has a significant effect on seismic data (Figure 5c). Although the two gathers exhibit similar characters, they differ significantly in both amplitude and phase (Figure 5c). For a slower source velocity, the differences are likely to be negligible for low frequencies; however, at high frequencies or for fast boat velocities, the source motion introduces artifacts if not properly taken into consideration in the processing workflow (Guitton et al., 2021).

Figure 6 shows traces from stationary and mobile acquisition correlated with the sweep. Here, we consider the case of correlating the sweep with traces from stationary acquisition as the reference. Correlating the sweep with near-offset traces from stationary and mobile acquisition produces similar results (Figure 6a). However, correlating the sweep with far-offset traces shows that a 1D assumption for correlation is no longer valid (Figure 6b). If source motion effects are not taken into consideration, correlating (or deconvolving) recorded data with the sweep causes artifacts in the processed data. Source movement poses other data processing and imaging challenges, that introduce interpretation uncertainties, as explained in a companion report.

5 DISCUSSION

Source motion introduces frequency shifts proportional to the boat velocity, acoustic wave velocity in the medium, propagation direction, and input frequency. The frequency shifts in the modeled seismic data are more noticeable at high frequencies, even with a slow source velocity. Neglecting frequency shifts and the time-dependent source-receiver offset in seismic data processing and imaging introduces significant artifacts in the processed data and ensuing imaging and/or inversion workflows. Although source motion causes noticeable frequency shifts in data, a change in source position when emitting is expected to have a more significant impact on seismic processing and imaging. Also, one can expect the source motion effects to be more significant for shallow targets than deep targets (Almuteri et al., 2022), and on far-offset traces than near-offset traces.

Our numerical results show that solving the second-order acoustic wave equation using a finite-difference approach with Taylor-expansion coefficients is accurate and stable. Adopting such an approach enables obtaining reliable subsurface images and reduces interpretation uncertainties. Although time-dependent meshes require repeated and expensive interpolation of the physical properties of the subsurface, the proposed work mitigates the need for such interpolations by using a judicious coordinate transformation to confine the mesh deformation to the homogeneous water layer. Also, the proposed methodology would help improve marine acquisition design and processing workflows by providing reliable and robust tools for numerical experimentation.

In conventional marine acquisition, source-side ghost reflections are described by an effective static sea surface (Blacquière and Sertlek, 2019), i.e. they occur instantaneously. However, for moving and long-emitting sources, source-side ghost reflections are explained using a dynamic sea surface model. Understanding the effects ghost reflections have on marine vibrator data is critical

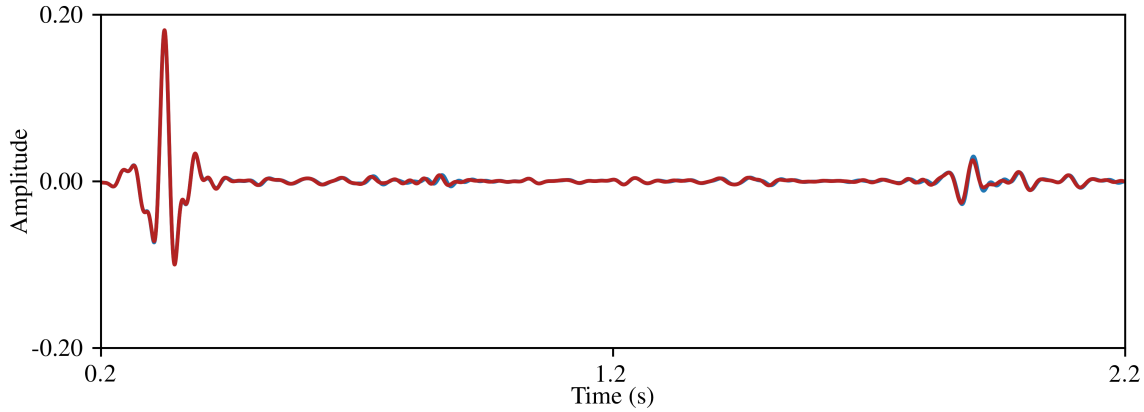

(a)

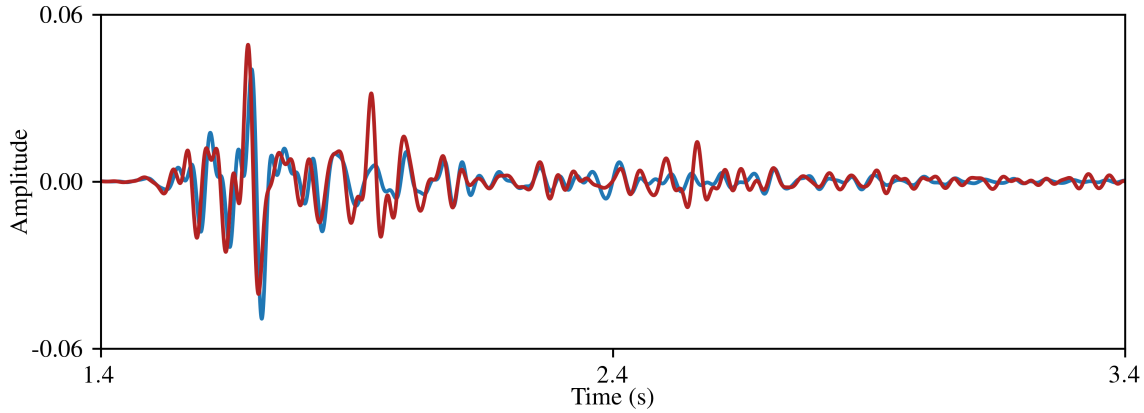

(b)

Figure 6. Traces recorded at receivers positioned at (a) x=8.5 km and (b) x=11 km. Blue and red traces are from stationary (Figure 5b) and mobile (Figure 5a) acquisition, respectively.

for developing robust seismic deghosting solutions for this type of acquisition. Therefore, future work involves incorporating a dynamic sea surface to mimic more realistic marine vibrator acquisition scenarios.

6 CONCLUSIONS

We present a finite-difference approach for solving the acoustic wave equation to simulate marine vibrator data. The developed method employs a geometric coordinate transformation to compute the full acoustic wavefield in a uniformly spaced and time-invariant mesh grid. Although our implementation assumes a source moving with a constant velocity, incorporating a variable velocity moving source in this framework is straightforward. The proposed numerical approach can accurately and stably model seismic wavefields even at unrealistically high velocities of the moving source. Further, this work is not limited to modeling marine vibrators, but can also be used to model towed-streamer data.

7 ACKNOWLEDGEMENTS

The first author would like to thank Saudi Aramco for graduate study sponsorship. We thank the sponsors of the Center for Wave Phenomena consortium at the Colorado School of Mines for the support of this research. We also thank Antoine Guitton from Total Energies for helpful discussions.

REFERENCES

Almuteri, K., P. Sava, and J. Shragge, 2022, Reverse-time migration of mobile marine vibrator data: CWP report, **1002**.

Bennett, J., 1968, The ray theory of Doppler frequency shifts: Australian Journal of Physics, **21**, no. 3, 259–272.

Blacquière, G., and H. Ö. Sertlek, 2019, Modeling and assessing the effects of the sea surface, from being flat to being rough and dynamic: Geophysics, **84**, no. 2, T13–T27. (doi:https://dx.doi.org/10.1190/geo2018-0294.110.1190/geo2018-0294.1).

Davies, K., 1965, Ionospheric radio propagation: US Department of Commerce, National Bureau of Standards, **80**.

Dellinger, J., and E. Díaz, 2020, Efficient modelling of extended-duration moving seismic sources: EAGE 2020 Annual Conference & Exhibition Online, European Association of Geoscientists & Engineers, 1–5. (doi:https://dx.doi.org/10.3997/2214-4609.202010838).

Doppler, C., 1842, Ueber das farbige licht der Doppelsterne und einiger anderer Gestirne des Himmels: Versuch einer das Bradley'sche Aberrations-Theorem als integrirenden Theil in sich schliessenden allgemeineren Theorie: K. Böhm Gesellschaft der Wissenschaften, 465–482.

Dragoset, W. H., 1988, Marine vibrators and the Doppler effect: Geophysics, **53**, no. 11, 1388–1398. (doi:https://dx.doi.org/10.1190/1.144241810.1190/1.1442418).

Duquet, B., A. Guitton, S. Secker, A. Feltham, and J.-P. Mascomere, 2021, Impact of non-impulsive moving source correction for structural and 4D imaging: First International Meeting for Applied Geoscience & Energy, Society of Exploration Geophysicists, 31–35. (doi:https://dx.doi.org/10.1190/segam2021-3594448.1).

Guitton, A., B. Duquet, S. Secker, J.-P. Mascomere, and A. Feltham, 2021, A deconvolution-interpolation approach with sparse inversion to mitigate the Doppler effect in marine vibrators data: First International Meeting for Applied Geoscience & Energy, Society of Exploration Geophysicists, 2555–2559. (doi:https://dx.doi.org/10.1190/segam2021-3593897.1).

Hampson, G., and H. Jakubowicz, 1995, The effects of source and receiver motion on seismic data: Geophysical Prospecting, **43**, no. 2, 221–244. (doi:https://dx.doi.org/10.1111/j.1365-2478.1995.tb00133.x).

JafarGandomi, A., and S. Grion, 2021, Modelling of marine vibrator data: 82nd EAGE Annual Conference & Exhibition, European Association of Geoscientists & Engineers, 1–5. (doi:https://dx.doi.org/10.3997/2214-4609.202113202).

Kolano, R. A., 1978, Doppler shift in layered media: Technical report, The Pennsylvania State University Institute for Science and Engineering - Applied Research Laboratory.

Konuk, T., and J. Shragge, 2020, Modeling full-wavefield time-varying sea-surface effects on seismic data: A mimetic finite-difference approach: Geophysics, **85**, no. 2, T45–T55. (doi:https://dx.doi.org/10.1190/geo2019-0181.1).

Laws, R., D. Halliday, J.-F. Hopperstad, D. Gerez, M. Supawala, A. Özbek, T. Murray, and E. Kragh, 2019, Marine vibrators: the new phase of seismic exploration: Geophysical Prospecting, **67**, no. 6, 1443–1471. (doi:https://dx.doi.org/10.1111/1365-2478.12708).

Schultz, P. S., A. W. Pieprzak, G. R. Johnson, and L. Walker, 1989, Simple theory for correction of marine vibroseis phase dispersion, *in* 59th Annual International Meeting: SEG, Expanded Abstracts, 660–662. (doi:https://dx.doi.org/10.1190/1.1889560).

Shragge, J., 2014, Solving the 3D acoustic wave equation on generalized structured meshes: A finite-difference time-domain approach: Geophysics, **79**, no. 6, T363–T378. (doi:https://dx.doi.org/10.1190/geo2014-0172.1).

Shragge, J., and B. Tapley, 2017, Solving the tensorial 3D acoustic wave equation: A mimetic finite-difference time-domain approach: Geophysics, **82**, no. 4, T183–T196. (doi:https://dx.doi.org/10.1190/geo2016-0691.1).

Weekes, K., 1958, On the interpretation of the Doppler effect from senders in an artificial satellite: Journal of Atmospheric and Terrestrial Physics, **12**, no. 4, 335–338.